www.sciencemag.org/content/351/6274/699/suppl/DC1

Supplementary Material for

A decade of sea level rise slowed by climate-driven hydrology

J. T. Reager,* A. S. Gardner, J. S. Famiglietti, D. N. Wiese, A. Eicker, M.-H. Lo

*Corresponding author. E-mail: john.reager@jpl.nasa.gov

Published 12 February 2016, *Science* **351**, 699 (2016)
DOI: 10.1126/science.aad8386

This PDF file includes:

Materials and Methods

1. GRACE JPL mascon solution over land

We use the JPL GRACE mascon solution (JPL RL05M) ***(36)***, from April 2002 through December 2014, which parameterizes monthly gravity field variations using 4,551 equal-area 3^{o} surface spherical cap mascons distributed globally. Analytical partial derivatives relating the surface spherical cap mascons to the inter-satellite range-rate measurements between the pair of GRACE satellites are used to estimate variations in the gravity field every month. The choice of the mascon basis function allows for convenient application of a priori information (which is derived from near-global geophysical models and ancillary observations) to remove correlated error in the gravity solution during the inversion. Implementation of time correlation in a Kalman filter approach reduces the solution dependency on the geophysical models to recover accurate mass variations, in particular trends. The resulting mass flux solutions are shown to suffer less from leakage errors than spherical harmonic solutions, and do not necessitate empirical filters to remove north-south stripes, lowering the dependence on scale factors (the global mean scale factor decreases by 0.17) to gain accurate mass estimates. Computing basin averages for hydrology applications shows general agreement between harmonic and mascon solutions for large basins; however, the mascon solution typically has greater resolution for smaller spatial regions, in particular when studying secular signals. This product was developed at the Jet Propulsion Laboratory, and is now available for public use on the GRACE Tellus website at grace.jpl.nasa.gov.

We perform standard modifications to the solution to correct for observational limitations of the GRACE satellites and limitations in the processing of the data. These modifications include replacing the degree 2, order 0 coefficients for each month with those estimated by a satellite laser ranging analysis (*38*), adding an estimate of geocenter motion (*40*), modifying the C_{21} and S_{21} coefficients to correct for the position of the mean

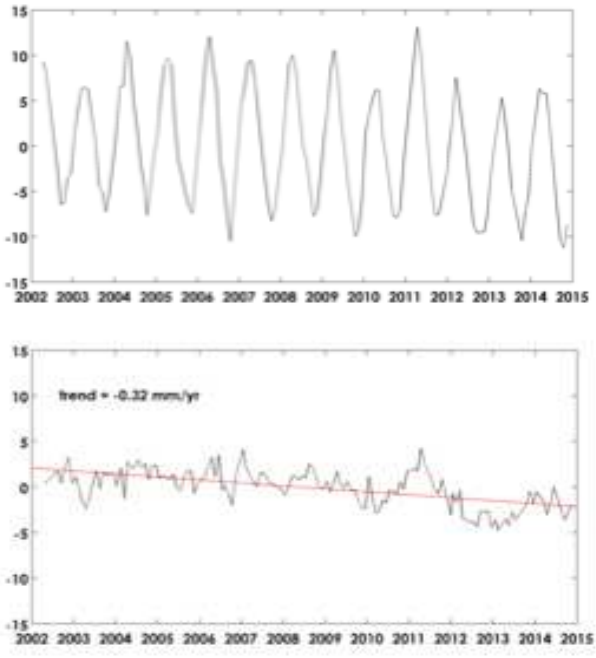

Figure S.1: (*top*) Full land mass anomaly time series; (*bottom*) Land time series with climatology removed, and a best-fit linear trend.

pole (*39*), and correcting for known atmospheric pressure jumps in the AOD1B RL05 background dealiasing model (*56*). To isolate the total land water storage (LWS) component of the GRACE gravity signal, we remove glacial isostatic adjustment (GIA) signals using the Paulson model (*57*) with the ICE-6G_C loading history (*37*), and tectonic signals caused by large earthquakes that GRACE was sensitive to (*41*). These corrections and their effect on the global land-mass trend are explained in detail in the following sections.

Systematic errors in mass trends arise from uncertainty in the GIA model, uncertainties in the glacier mass change signal, uncertainty in the geocenter correction, uncertainty in the mean pole correction and uncertainty in the earthquake correction. To produce our land (all continents except Antarctica and Greenland) water storage (all snow, surface water, soil water and groundwater, but excluding glaciers) signal, these corrections introduce additional uncertainties into the trend estimation, each of which is discussed in detail below. Formal GRACE solution errors originate from signals outside the area of interest leaking into the regional solution spatially, and from attenuation of the signal related to the sensitivity of the instrument (*58*). Averaging over all land globally and propagating into a 140-month trend fit, this error is below the precision of the uncertainties in the corrections.

Figure S.1 shows the GRACE total land mass time series (excluding only Greenland and Antarctica), representing an observational estimate of the total net mass exchange between the global land and ocean at monthly resolution from 2002 to 2014. We find this signal has annual peak-to-peak amplitude of 17.3 +/- 3 mm SLE, estimated by calculating a monthly climatology of land mass anomaly. Removing the climatology, and fitting a linear trend by a least-squares approach, we estimate a global continental land mass trend of -0.32 mm yr^{-1} SLE (i.e. sea level rise). We test the sensitivity of this trend to each of the applied corrections in the following sections.

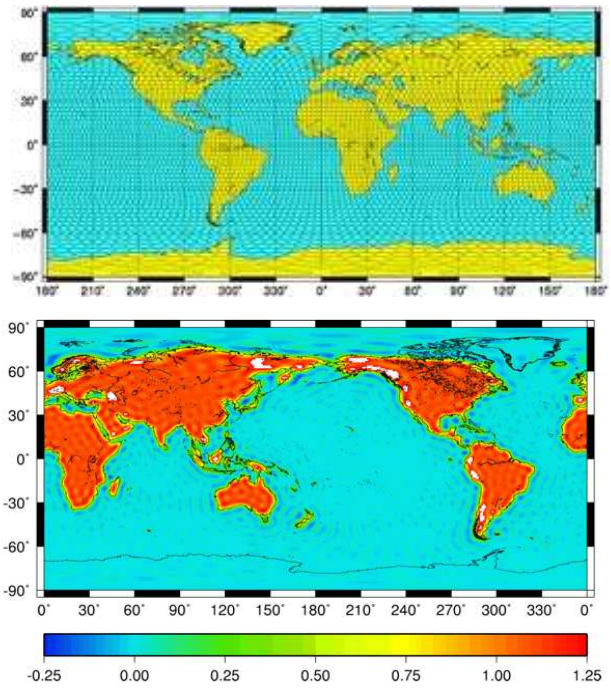

Figure S.2. (*top*) mascon placement in the JPL RL05M mascon solution. (*bottom*) Dimensionless averaging function used to estimate the terrestrial water storage changes from GRACE spherical harmonic data for the global land. White areas represent coastal glaciated regions and are scaled by a factor of 1.7.

1.1. Comparison of mascon solution with spherical harmonic solution

Correcting for leakage errors is extremely important when calculating mass balances for regions on land/ocean boundaries, and is one of the primary differences between the

new mascon approach and the standard spherical harmonic solution. The mascon solution has leakage errors to the extent that some of the mascons are geophysically located on coastlines, so the observed mass is a mix of land and ocean signals. To reduce this leakage error we apply a Coastline Resolution Improvement (CRI) filter to separate between land and ocean mass within mascons that span coastlines. This filter uses statistical information from ocean and hydrology models to perform the disaggregation, and has been shown to reduce leakage errors by more than 50% globally (*36*).

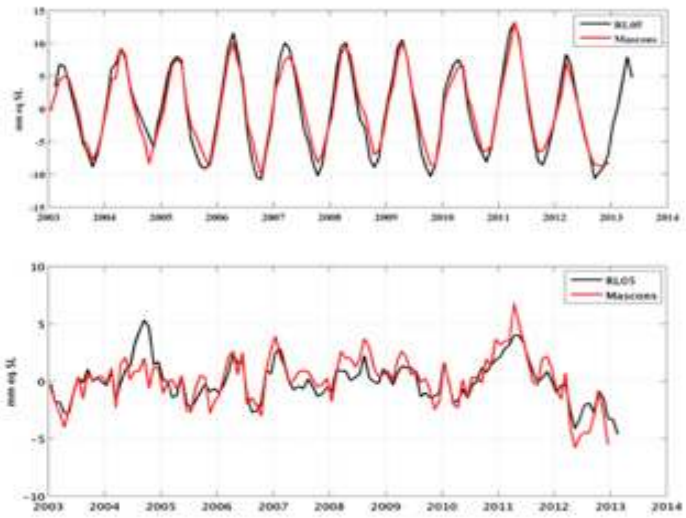

Figure S.3: Mascons vs. spherical harmonics timeseries with (*top*) full signal over land and (*bottom*) climatology removed. "RL05" refers to the JPL RL05 spherical harmonics, and "mascons" refers to the JPL RL05M mascons.

Since this approach to reducing leakage errors between land and ocean is novel (as is the development of the mascon solution itself), we compare mascon results with global land mass time series produced by applying an averaging-kernel (Figure S.2) to the JPL Release 5.0 spherical harmonic solution. All of the processing corrections are applied to the spherical harmonic and mascon solutions equally.

Time series for the two approaches are compared in Figure S.3, with and without the seasonal climatology included. There is strong agreement between the two time series for both cases; with only small deviations at higher-frequencies indicating that land-ocean partitioning has little overall impact on the global land mass trend.

1.2. Geocenter correction

A geocenter motion correction (degree one spherical harmonic coefficients) is applied according to *Swenson et al.* (*40*). This method estimates the time evolution of geocenter anomalies using data from GRACE and output from an ocean model. Results have been compared to independent estimates of geocenter derived from other satellite data, such as satellite laser ranging and GPS. The estimated degree one coefficients are used to improve estimates of mass variability from GRACE since the satellites are insensitive to this term as they orbit the center of mass of the Earth.

Figure S.4 shows the spatial pattern of the isolated geocenter trend signal over land as well as the time series of the geocenter correction over land. The geocenter signal (which is added to the GRACE solution) is negative in the northern hemisphere and positive in

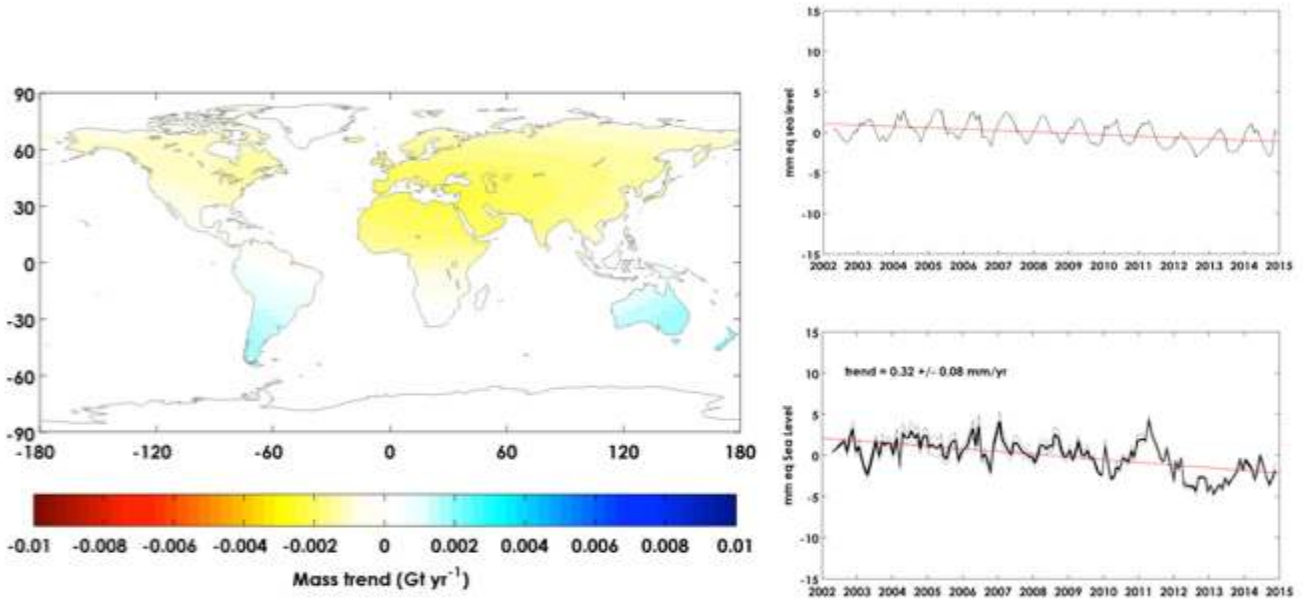

Figure S.4: Geocenter correction and the effect on the global land mass trend. (*left*) The map of geocenter trend over land (note finer-scale color axis); (*top right*) the time series of geocenter-caused mass change over land; (*bottom right*) the total land mass time series with +/- 50% adjustment of the geocenter signal.

the southern, resulting in a net negative mass trend over land of -58 Gt yr^{-1}, equivalent to 0.16 mm yr^{-1} SLE (i.e. ocean gaining), but also possesses strong seasonal periodicity. To investigate the uncertainties in estimated geocenter motion, we compare the applied correction to two other independently derived estimates. *Rietbroek* (*35*) compute geocenter motion with a joint inversion scheme using GRACE and satellite altimetry observations and *Wu et al.* (*59*) apply a combination of GRACE observations, GPS surface displacements, and ocean model output. The standard deviation of the land mass contribution of the three estimates amounts to 0.05 mm yr^{-1} SLE, which corresponds to ~30% uncertainty. We conservatively assign an uncertainty of +/- %50, or +/- 0.08 mm yr^{-1} SLE to the geocenter trend. This uncertainty contributes 25% of the total uncertainty budget on the GRACE land mass trend.

1.3 Mean pole correction

The pole tide is defined as the response of the solid Earth and oceans to polar motion. It causes gravity signals that manifest in low spatial harmonics, typically of degree 2, order 1. The pole tide affects the coefficients of those harmonics ($C21$, $S21$) if it is not removed, and introduces errors when using those coefficients to determine surface mass variations caused by changes in hydrology. Long-period pole tide signals are not usually included in the GRACE pole tide correction, and so those signals are still present in the GRACE coefficients, and can manifest in a trend analysis. *Wahr et al.* [2015] recommend modifying the $C21$, $S21$ coefficients to achieve an optimal GRACE pole tide correction.

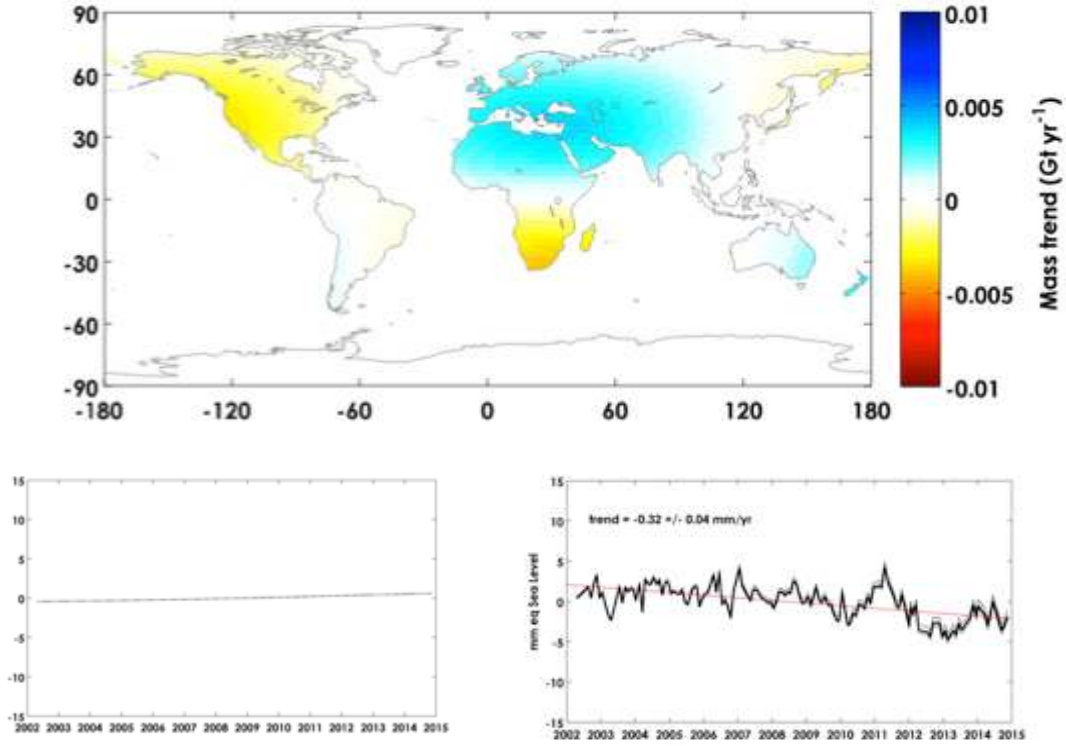

Figure S.5: Mean pole correction and its effect on the global land-mass trend. (*top*) The mass trend over land caused by *Wahr et al.'s* (*39*) recommended correction; (*bottom left*) the trend over land as a time series in mm yr^{-1} SLE; (*bottom right*) the effect of a +/- 50% adjustment in the meanpole signal on the total land mass time series (climatology removed).

To investigate the effect of the mean pole trend on the land mass trends, we assume an uncertainty on the *Wahr et al.* (*39*) recommended mean pole correction over land of +/- 50%. Figure S.5 shows the spatial pattern of the isolated mean pole trend signal over land as well as the time series over land in units of SLE. The mean pole signal is a cumulative positive mass trend over the continents, mostly negative in North America, and positive in Eurasia and Northern Africa. This signal (which is subtracted from GRACE) corresponds to a land mass trend of 29 Gt yr^{-1}, or approximately -0.08 mm yr^{-1} SLE (i.e. land gaining), and a 50% uncertainty represents a +/- 0.04 mm yr^{-1} variation around that signal. This uncertainty contributes ~12% of the total uncertainty budget on the GRACE land mass trend.

1.4. GIA correction

Here we use the recently published estimates of ICE-6G_C (VM5a) that are described in *Peltier et al.* (*37*). The ICE-6G_C loading history model is constrained by GPS measurements of vertical displacement for the period 1994-2012, augmented by additional space geodetic constraints. This strategy has led to a significant improvement over the previous model ICE-5G (VM2), and the improvement of the fit provided by ICE-6G_C (VM5a) over the other models is especially evident for North America [*c.f.*

Peltier et al., (*37*) Figure 5]. The new model also does well over Fennoscandia [*c.f. Peltier et al.,* (*37*) Figure 12]. In both regions a suite of comparisons of the predictions of the new and old models to relative sea level histories were performed (*37*).

There is no formal uncertainty provided with ICE-6G, or any other available estimates of GIA uncertainty that we are aware of. To explore effects that GIA uncertainty may have on our assessment of global hydrology trends, we examine the spread between three global GIA models and use this as a best-estimate of the uncertainty introduced by the GIA correction. These models are based on a reconstruction of ice loading histories and the predicted crustal response. The models used include: (1) ICE-6G_C loading history and VM5a viscosity profile (*37*); (2) ICE-5G loading history and Paulson viscosity profile (*57,60*); and (3) ICE-5G loading history and VM2 viscosity profile (*61*). This set

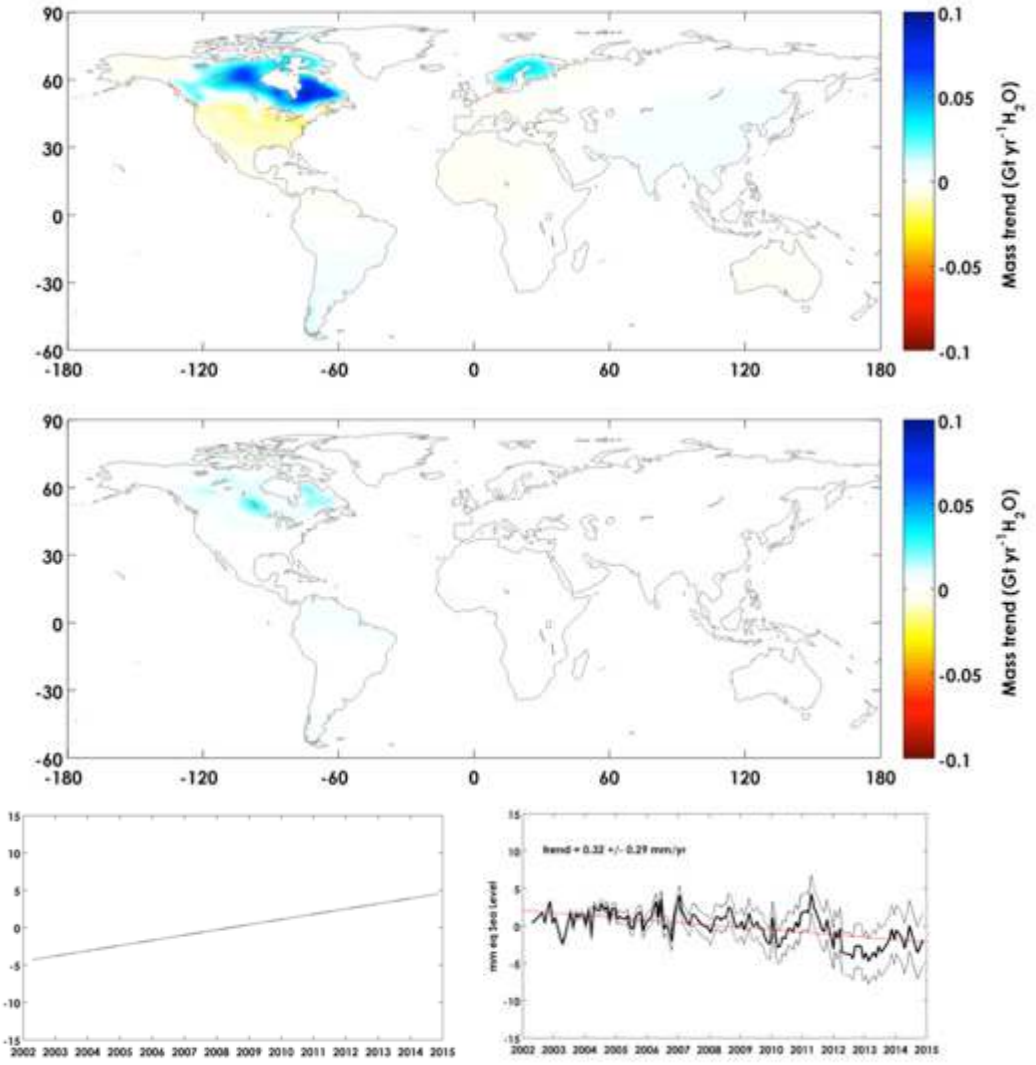

Figure S.6: GIA correction and its effect on the global land mass trend. (*top*) The map of the ICE-6G mass change estimates over land; (*middle*) the map of the standard deviation of the three GIA models used; (*bottom-left*) the trend in GIA over land in mm yr^{-1} SLE; (*bottom-right*) the effect of a +/- 50% adjustment in the GIA correction on total land mass (climatology removed).

represents two distinct glaciation histories and two distinct viscosity profiles.

Figure S.6 shows the ICE-6G (VM5a) modeled GIA signal, as well as the standard deviation between the 3 models. The largest deviation in the domain is located in the border between signals of opposite sign in North America. We adopt the 3-sigma spread between the global land mass trends for the three GIA models as the uncertainty in the ICE-6G GIA correction. We consider this a conservative estimate as *Peltier et al.,* (*37*) convincingly demonstrate improved agreement of ICE-6G to observations (gravimetry and vertical crustal displacement) over earlier models. From this approach we determine an uncertainty of +/- 0.08 mm/yr SLE. This number represents about ~25% of the total land mass trend error budget.

1.5. Tectonic signals over land in GRACE

As part of the gravity field observed by GRACE, earthquakes cause variations in the gravitational potential field at a spatial scale up to some thousands of kilometers and at temporal scales of seconds to decades, by radiating seismic energy and deforming the surface and interior (*41*). Tectonic signals therefore must be removed from the GRACE observations to isolate the hydrology signal.

We remove the effect of three seismic events from the GRACE record: the 2004 Sumatra-Andaman earthquake, the 2010 Maule earthquake, and the 2011 Tohoku-Oki

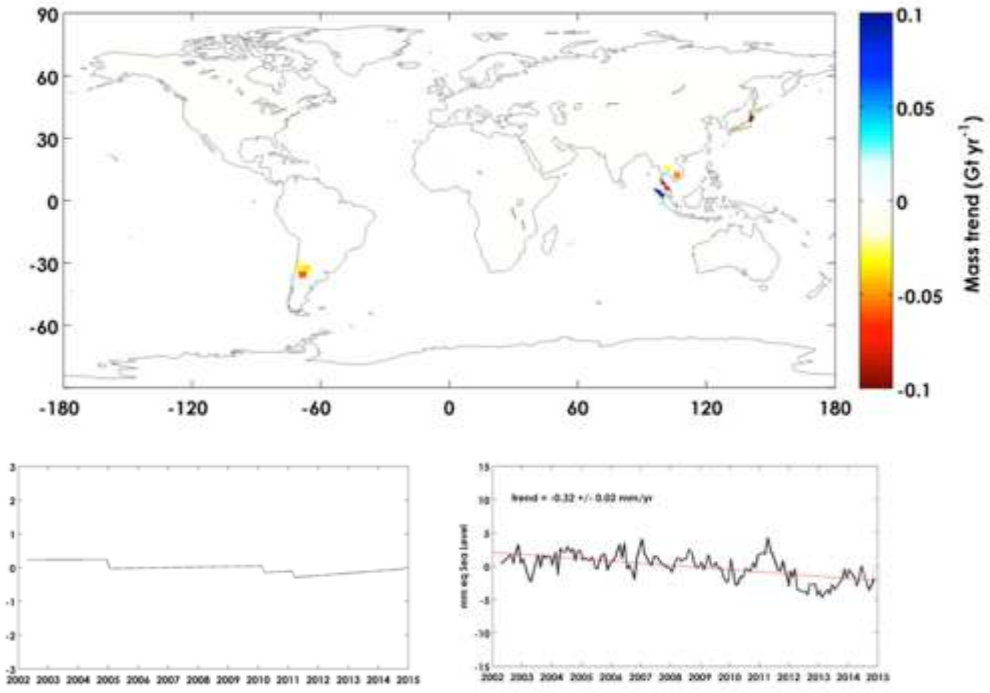

Figure S.7: Tectonic corrections and their effect on the global land-mass trend. (*top*) The map of mass trends caused by tectonic signals over land; (*bottom-left*) the time series of tectonic activity in mm yr^{-1} SLE (note y-axis change); (*bottom-right*) the effect of a +/- 50% adjustment of the tectonic signal on the total land mass time series (climatology removed).

earthquake, as these were all substantial enough in magnitude to be observed by GRACE (*41*). We use the models of Han et al., (*41*) to geospatially locate mascons which capture the earthquake signals, and then fit a Heaviside function at the earthquake epoch to account for the coseismic response, followed by a linear trend in the months after the earthquake to account for the postseismic relaxation. While a linear trend may not be the best parameterization for the postseismic response, models do not currently exist for this behavior, and we consider this to be a conservative approach for our analysis. Fortunately, these three large earthquakes predominately occurred over the ocean, so there is little contamination of land hydrology signals (Figure S.7). Additionally, it is seen that most of the contamination of land hydrology is due to the coseismic event rather than the postseismic relaxation.

The cumulative tectonic motion during the study period contributes 0.04 mm yr^{-1} SLE to the continents (land mass gain). Because of a lack of observations to constrain the uncertainty in this estimate we adopt a conservative uncertainty of +/- 50% of the total signal. This results in a +/- 0.02 mm yr^{-1} uncertainty on the global land mass trend, representing ~7% of the error budget for the global land mass trend.

1.6. Glacier signals

Mass loss from glaciers is currently the largest transfer of mass from land into the oceans. Here we estimate a glacier correction that can be applied to the JPL mascon trends in continental mass storage to isolate mass anomalies in terrestrial water storage. We do this using three separate approaches:

1. For those mascons with large concentrated glacier coverage, where mass trends are dominated by changes in glacier mass, we assign a zero trend in terrestrial water storage and add additional uncertainty to the land water storage (LWS) signal. We apply this approach for Alaska, Arctic Canada North, Arctic Canada South, Iceland, Svalbard, Russian Arctic Islands, and the Southern Andes regions as defined by the Randolph Glacier Inventory (*62*). This approach minimizes errors introduced from uncertainties in Little Ice Age and GIA signals that would be required to separate solid earth and glacier signals within these mascons. As a sanity check we compare mass trends for these mascons against the published values in *Gardner et al.* (*10*) for the matching period 2003 to 2009. Using the same LIA and GIA corrections as applied in *Gardner et al.,* (*10*) we get good agreement with their published values to within +/- 5 Gt yr^{-1} for all regions. To estimate the error introduced by setting the LWS trend in these mascons to zero we assign an uncertainty to these mascons equal to two times the standard deviations in LWS trends for all other land mascons (2 × 8.6 mm w.e. yr^{-1}) scaled by the area of glacier free terrain within each mascon. Taking this approach has little effect on the estimated trend in LWS. As an example, if the real LWS anomaly for all 125 million km^2 of glacier free terrain within these glacier mascons was 10 times the global average trend in LWS (0.96 kg m^{-2} yr^{-1}) this would result in a trend of 0.05 mm yr^{-1} SLE, well within the uncertainty of our analysis.

Table S.1: Glacier trend estimation showing region, area, time period, data source, corrections applied and trend and uncertainty estimates.

Region	Glacier Area [km^2]	Period	Source	TWS Correction includes	TWS Correction dM/dt ± 2σ [Gt/yr]	GIA ± 2σ [Gt/yr] (G13)	LIA ± 2σ [Gt/yr] (J12)	Glacier only dM/dt ± 2σ [Gt/yr]
Alaska	87100	2002-14	JPL Mascons	glacier, GIA, LIA	-52.0 ± 12	+1 ± 2	-7 ± 4	-58.5 ± 12.8
Western Canada and USA	14600	2002-12	GMBAL	glacier only	-13.3 ± 5.7	-5 ± 14	-0 ± 0	-13.3 ± 5.7
Arctic Canada North	104900	2002-14	JPL Mascons	glacier, GIA, LIA	-39.0 ± 4.1	-3 ± 2	-0 ± 0	-42.0 ± 4.5
Arctic Canada South	40900	2002-14	JPL Mascons	glacier, GIA, LIA	-35.6 ± 5.1	-5 ± 6	-0 ± 0	-40.6 ± 7.9
Iceland	11100	2002-14	JPL Mascons	glacier, GIA, LIA	-8.8 ± 1.2	-0 ± 0	-0 ± 0	-8.8 ± 1.2
Svalbard	34000	2002-14	JPL Mascons	glacier, GIA, LIA	-4.8 ± 0.5	-2 ± 4	-0 ± 0	-6.8 ± 4.0
Scandinavia	2900	2002-12	GMBAL	glacier only	-3.0 ± 2.3	-5 ± 4	-0 ± 0	-3.0 ± 2.3
Russian Arctic	51600	2002-14	JPL Mascons	glacier, GIA, LIA	-4.9 ± 1.0	-5 ± 8	-0 ± 0	-9.9 ± 8.0
North Asia	3400	2002-12	GMBAL	glacier only	-0.7 ± 0.8	-1 ± 0	-0 ± 0	-0.7 ± 0.8
Central Europe	2100	2002-12	GMBAL	glacier only	-2.9 ± 1.1	-0 ± 0	-0 ± 0	-2.9 ± 1.1
Caucasus and Middle East	1100	2002-12	GMBAL	glacier only	-0.3 ± 0.1	-	-	-0.3 ± 0.1
High Mountain Asia	118200	2003-09	G13, Table S5	glacier only	-29.0 ± 26.8	-6 ± 4	-3 ± 1	-29 ± 26.8
Low Latitudes	4100	2002-12	GMBAL	glacier only	-2.2 ± 1.3	-0 ± 2	-0 ± 0	-2.2 ± 1.3
Southern Andes	29300	2002-14	JPL Mascons	glacier, GIA, LIA	-20.1 ± 10	-4 ± 2	-9 ± 5	-33.1 ± 12.1
New Zealand	1200	2002-12	GMBAL	glacier only	-1.9 ± 1.9	-0 ± 0	-0 ± 0	-1.9 ± 1.9
Total					-218.5 ± 32.7			-253.0 ± 35.4

Note: Error for mass changes determined from the JPL Mascons are taken to be 2 times the standard deviation of the trend in TWS for all non-glacierized mascons (2 × 8.6 mm w.e.) times the area of ice free terrain within each mascon. GMBAL (Cogley, 2009) errors are taken directly from data provided to the authors by G. Cogley. For High Mountain Asia we use the mass change estimates presented in Gardner et al., 2013 Table S5 and scale their error by a factor of two to account for differences in study periods. Error between regions are assumed random and propagated as the root sum of squares. G13 referes to Gardner et al. 2013 and J12 referes to Jacob et al. 2012.

2. For the high mountain Asia region, where changes in terrestrial water storage are known to be large (*e.g. 29*) and regional estimates of glacier mass change from the interpolation of in situ observations are known to be biased (*c.f.* Figure 3 of *Gardner et al.* (*10*)) we rely on estimates derived from satellite laser altimetry (ICESat) for the period 2003 to 2009 that are presented in Table S5 of *Gardner et al.* (*10*) which gives a total glacier mass change for the region of -29 ± 13.4 Gt yr^{-1}. We spatially distribute the glacier mass changes by multiplying the glacier areas within each mascon by the average rate of glacier loss for the three sub regions of Central Asia (-167 kg m^{-2} yr^{-1}), South Asia West (-202 kg m^{-2} yr^{-1}) and South Asia East (-513 mm kg m^{-2} yr^{-1}) as defined in RGI 3.0 (*62)*. To account for differences in study periods we scale the total uncertainty for the 2003-2009 period by a factor of two to give an uncertainty in the glacier correction for this region of 26.8 Gt yr^{-1}.

3. For all other glacierized regions, LWS signals likely dominate regional mass trends and solid earth response due to unloading of LIA ice is expected to be small. For these regions we remove the glacier signal using Release 1301 of the global analysis of the mass-balance dataset GMBAL adding the corresponding uncertainty in the glacier loss to our calculation of the trend in LWS. Details on GMBAL dataset can be found in *(63)*.

Glacier mass trend corrections for each glacierized region and respective uncertainties are provided in Table S.1 and Figure S.8. Our estimate of glacier change for the 2002-2014 period of -253 ± 35 Gt yr^{-1} agrees within error to *Gardner et al.*'s (*10*) estimate of -215 ± 26 Gt/yr for the period 2003-2009 (excludes Greenland and Antarctic periphery). Much of the difference between estimates can be attributed to slight higher rates of ice loss for Canadian Arctic North, Canada Arctic South and Russian Arctic regions during the last five years of the 2002-2014 record.

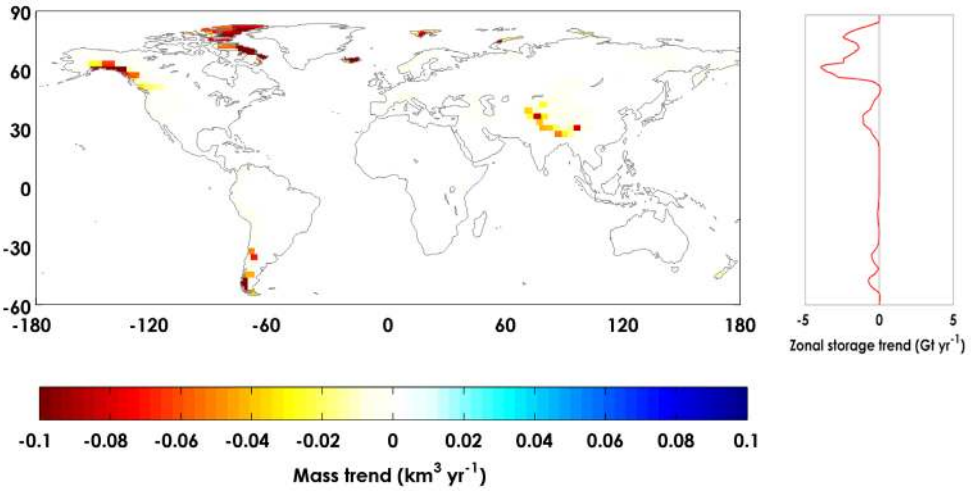

Figure S.8: Glacier correction and its effect on the global land mass trend. Map of the mass changes caused by glacier losses over the 2002-2014 study period in Gt yr^{-1} per mascon; a zonal average of glacial mass trends in Gt yr^{-1}.

1.7. Error budget

We determine the uncertainty in our LWS trend by propagating the error as the root sum of squares of the geocenter correction, mean pole correction, earthquake correction, GIA correction and the glacier correction. Note that there are formal errors associated with the GRACE monthly solutions themselves. Typically, these errors are approximately 2 cm of equivalent water height over 400 km spatial scales. However, once we average over land regions and propagate this error into a trend error, it becomes negligible, and as such, is disregarded from this analysis.

Table S.2: Budget of corrections and uncertainty applied to the GRACE data to yield an estimate of global hydrology trends. LIA and glacier signals are estimated concurrently for each glacier region. The errors marked with "*"only appear after their separation for this table and are propagated through the budget for land water storage as a combined correction.

Correction	**Trend (mm yr^{-1} SLE)**	**Uncertainty (mm yr^{-1} SLE)**
Geocenter motion	+0.16	+/- 0.08
Mean pole trend	-0.08	+/- 0.04
GIA	-0.58	+/- 0.08
Earthquakes	-0.04	+/- 0.02
Glacial mass loss	+0.70	+/- 0.10*
LIA	-0.05	+/- 0.07*
Sum of corrections (not including glacier and LIA)	**--**	**+/- 0.13**
Removing glaciers	**--**	**+/- 0.16**

2. Global mass budget closure and validation

Global mass budget closure is imposed in the formulation of the JPL RL05M mascon solution (as well as GRACE spherical harmonic solutions). Additionally, global mass budget closure is imposed in the derivation of the ICE-6G GIA model. These two constraints guarantee global mass budget closure. Table S.3 shows derived trends from non-ice sheet land areas (for which this study is focused on), as well as the derived trends for the global ocean, Greenland, and Antarctica. The sum of each of these components is equal to zero, meaning that global mass is conserved.

Table S.3. Trends (units of mm yr^{-1} SLE) derived from the JPL RL05M GRACE solution (after removal of GIA using ICE-6G) demonstrating global mass budget closure.

Term	2002-2014 Mass trend
Non-ice sheet land	-0.32
Oceans	1.58
Greenland	-0.77
Antarctica	-0.49
Sum	**0**

Numerous studies have been devoted to deriving individual components of the global mass budget shown in Table S.3; however, studies rarely consider each of these terms in concert with each other. For validation purposes, the following subsections of text are devoted to comparing our derived mass trends with published results.

2.1 Non-ice sheet land

For validation of our derived trend for non-ice sheet land areas, we compare our mascon-based land mass time series with the land mass trends published in previous studies. Figure S.9 shows the mascon global land mass time series, with trends fit over two distinct periods. First, we fit a trend over the same period (i.e. August 2002 to July 2009) as those fit by Llovell et al. (*34*) (0.22 +/- 0.05 mm yr^{-1}), Jensen et al. (*6*) (0.20 +/- 0.04 mm yr^{-1}), and Riva et al. (*43*) (0.10 +/- 0.3 mm yr^{-1}). We estimate a trend during this timeframe from the JPL RL05M mascon solution of 0.25 +/- 0.05 mm/yr, which agrees within uncertainty with each of these published estimates. This agreement validates both the data and methods that were used in this study to derive the estimated land mass trend of -0.32 mm yr^{-1} over the full timespan of April 2002 – November 2014.

This comparison highlights the sensitivity of mass trends estimated over short (i.e. less than ten-year) time periods. Additionally, we make no statements about the extrapolation of these trends beyond the observational period and in fact suggest that the land hydrology 'trend' presented here may be due to decadal-scale variability, and could change substantially in the future, with implications to the sea level budget.

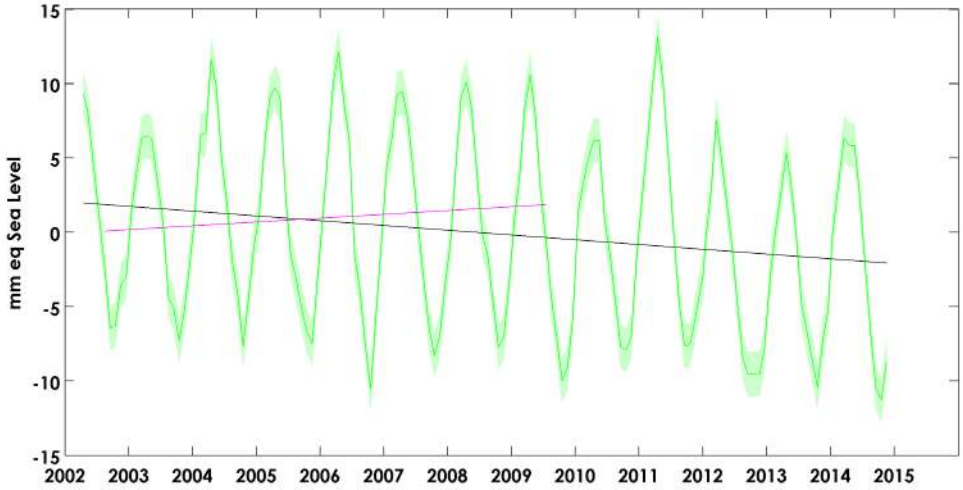

Figure S.9 : The GRACE mascons were applied to estimate global land mass trends during the August 2002 to July 2009 time period, following previous studies. We find a trend using the mascon solution that is consistent with earlier studies (+0.25 mm yr^{-1}). For the full record, we estimate a trend of -0.32 mm yr^{-1} .

2.2 Global oceans

We estimate a global ocean mass trend of 1.58 mm yr^{-1} over the full time period of this study (Table S.3). For validation of our data and methods, Figure S.10 shows the global ocean mass timeseries with two distinct trends fit to the data. The first is for the full length of the data record (1.58 mm yr^{-1}), and the second is from Jan 2005 – Dec 2014 (2.0 mm yr^{-1}), selected to match that of Llovel et al. (*44*). The Llovell et al. (*44*) estimate is an important comparison because they demonstrate global sea level budget closure over their period of study. Using the GRACE estimates of mass change and the ARGO estimates of thermal expansion, they were able to match global altimetry estimates of sea level rise. Llovel et al. (*44*) found that the global ocean mass was increasing at a rate of 2.0 mm yr^{-1} from 2005 to 2014. We exactly reproduce this result when using a coincident time period. This gives us confidence that our derived global ocean mass trend should also achieve sea level budget closure over the longer timeframe of this study (although this work is not presented in this manuscript as it is out of the scope of the study). Similar to the results for the non-ice sheet land areas, we find the derived trend is quite sensitive to the selected time period, again warranting caution when comparing trends fit over differing short intervals.

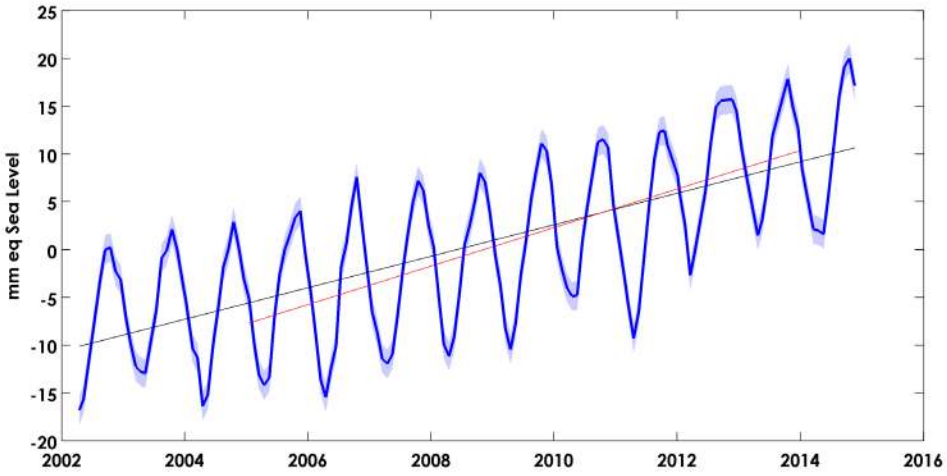

Figure S.10: The GRACE mascons were applied to estimate global ocean mass trends for two time periods: The 2005-2013 time period (following Llovell et al., (*44*)) and the full record (April, 2002 to November 2014). We find a trend using the mascon solution that matches identically with the Llovel et al. (*44*) estimates of 2.0 mm yr^{-1} mass gain over the 2005-2013 period. For the full record, we estimate a trend of 1.6 mm yr^{-1}.

2.3 Greenland and Antarctica

Rather than validating our data and methods over Greenland and Antarctica explicitly here, we direct the curious reader to Table 4 in *Watkins et al.* (*36*) where a comparison between eight independent studies and the JPL RL05M mascon solution is made over differing study time periods. That analysis shows that the mass trend for Greenland derived from the JPL RL05M solution (including the GIA correction) agrees with all studies within formal uncertainties, and particularly well with *Sasgen et al*. (*64*), to within 3 Gt yr^{-1}, as well as *Schrama et al*. (*65*), to within 7 Gt yr^{-1}. For Antarctica, the inter-study comparison is made independent of the GIA correction; that is, it tests only the processing and interpretation of the GRACE data. Again, the JPL RL05M solution is found to agree within formal uncertainties, and best with *Sasgen et al*. (*66*), to within 5 Gt yr^{-1}. Significant uncertainty is introduced in the application of the GIA correction for Antarctica as discussed in Shepherd et al. (*11*). This primarily explains the differing rate of mass loss we observe for Antarctica with respect to what is published in *Shepherd et al.* (*11*), where regional GIA models were used to calculate the Antarctica mass trend rather than the global mass-conserving model (ICE-6G) we have used.

In summary, the data and methods presented here lead to global mass budget closure. Results presented here are validated with comparisons to previously published estimates for non-ice sheet land areas, global ocean mass, Greenland, and Antarctica. The largest disagreement with previously published results and our estimates come in Antarctica, which is largely attributed to differences in GIA models used for those regions and has little impact on the results and conclusions of this study which only focuses on the trend in terrestrial water storage.

3. Comparative analysis of results

3.1. Precipitation

For mass to increase over land (i.e. a trend in storage or a positive *dS/dt*), there needs to exist a change in the fluxes of precipitation, evaporation or runoff relative to one another. This would not necessarily manifest as trend in precipitation or another single flux over the study period, given, for example, the case of a change in the mean rates relative to one another. Global runoff and land evapotranspiration are difficult to estimate observationally. To investigate the possibility of a concurrent signal in precipitation observations, we apply data from the Global Precipitation Climatology Project (GPCP) (*67*), noting that this comparison alone only suggests a possible mechanism for the observed land mass changes.

The spatial pattern of this trend is shown in Figure S.11. These trends in precipitation generally support the hypothesis of increasing land hydrology mass over the GRACE record for several regions, including the Amazon and North Eastern Australia. It is possible that in other regions, recovery from drought periods preceding the GRACE record, flood events, or increases in seasonal (e.g. snow) precipitation could drive a trend in storage without showing a trend in precipitation over the entire study period.

Generally, interannual variations in storage are modulated by interannual variations in the water balance (i.e. the residual of precipitation, evaporation and runoff fluxes). Global land precipitation increases of 0.69 +/- 0.12 km^3 day^{-1} yr^{-1} were observed for a subset of the study period (from 2003-2012) based on data from GPCP. An increased flux of this magnitude would have delivered an additional 3000 +/- 500 Gt of water to land, roughly equivalent to the observed climate-driven land mass trend. The largest increase in precipitation during the study period coincided with the well-documented 2011 La Niña event, which acted to deliver extra water to Australia, North America and the Amazon (*21,50*). Excess precipitation that recharges aquifers and soils can remain in storage for subsequent years. During long periods of anomalous precipitation, the land can generally be wetter (drier) than normal, and less (more) water is stored in the Oceans (*33*). These variable periods are amplified by changing human water use (*e.g.* groundwater pumping or reservoir storage) (*17*).

Our results suggest interesting processes for further exploration. The terrestrial hydrological cycle exhibits strong interannual and decadal variations (*44,68*), and trends in land hydrology (i.e. ground water, soil water, and snowpack) are likely driven by internal variability in the climate system. Recent analysis of a global warming "hiatus" and a corresponding increasing contrast in land and ocean temperatures (*e.g. 69*) form complimentary evidence for intensification of ocean-land water vapor transport during the GRACE period. It is entirely feasible that this variability could reverse directions, causing a decadal increase of the sea level trend.

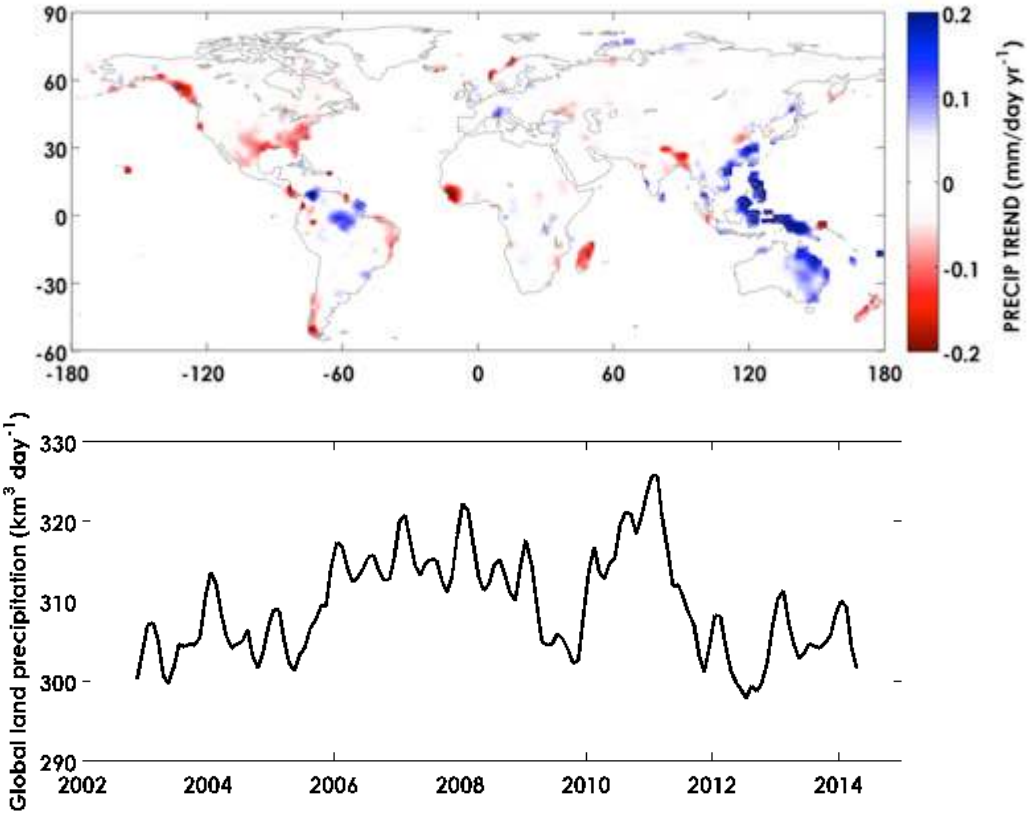

Figure S.11: Precipitation trends over the April 2002 to November 2014 study period from Global Precipitation Climatology Project (GPCP)

3.2. Human-induced changes in hydrology

Much work has been performed on estimating the direct human hydrology contributions to sea level change, which include groundwater pumping, reservoir construction and sedimentation, wetland drainage and deforestation. A survey of recent literature on this topic produces a range of possible values, each estimated using different methodological assumptions. For instance, using flux-based model estimates, *Wada et al.* (*13*) estimated a rate of groundwater depletion of 0.57 ±0.09 mm yr^{-1} in the year 2000. *Konikow* (*14*) estimated a global groundwater depletion of 0.41 ± 0.1 mm yr^{-1} for 2000-2008. The later estimate used in-situ groundwater storage with a model and GRACE satellite data to calculate depletion for the USA and five other major aquifer systems (north India, North China Plain, Saudi Arabia, Nubian and Sahara) that was then extrapolated globally. *Döll et al.* (*16*) used the WaterGAP hydrology model to estimate a contribution from groundwater depletion of 0.31 mm yr^{-1} (no uncertainty provided) during 2000-2009. In summary, previous work suggests that in the years after 2000, a range of possible values exists for groundwater contributions to sea level rise ranging from 0.31 to 0.57 mm yr^{-1}.

Richey et al. (*17*) present an estimate of depletion in the world's 37 largest aquifers based on the GRACE 'sub-surface' signal in each aquifer region. This was calculated by removal of snow and surface water storage terms, and the residual is assumed to represent changes in soil and ground water storage over the GRACE record. Since the study was conducted over aquifer regions, it is assumed to be correlated with human activity, though no human fluxes are explicitly calculated. We can apply the numbers from *Richey et al.* (*17*) as a compliment to the groundwater deletion estimates over the study period, though GRACE only sees changes in the net water storage, including both depletion and recharge. To achieve a global estimate of potential sea level contributions, we only consider the depleting (i.e. negative storage trend) signals from *Richey et al.* (*17*). These are listed in the Table S.3. We acknowledge that this is not an estimate of global groundwater depletion or consumption – it is a net value that includes natural groundwater recharge and climate-driven processes as well over aquifers, but serves as some evidence that human activities are offset by natural recharge.

Table S.4: Sub-surface water storage change for the global depleting aquifers over the study period, estimated by removing model estimates of snow and surface water storage from GRACE total water storage anomalies. After *Richey et al.,* 2015.

Aquifer name	Area (km^2)	Sub-surface trend (mm yr-1)	Sub-surface trend (km^3 yr-1)	Sub-surface error (km^3)
Arabian Aquifer System	1,700,712	-9.13	-15.53	1.53
Ganges-Brahmaputra Basin	621,564	-19.564	-12.16	0.76
Russian Platform Basins	2,753,613	-4.011	-11.04	2.91
Congo Basin	1,480,136	-4.848	-7.18	1.4
Atlantic and Gulf Coastal Plains Aquifer	1,143,928	-5.932	-6.79	1.16
Nubian Aquifer System	2,093,788	-2.906	-6.08	1.85
West Siberian Basin	2,623,196	-1.978	-5.19	2.6
North Caucasus Basin	260,250	-16.097	-4.19	0.37
Canning Basin	380,872	-9.41	-3.58	0.51
North China Aquifer System	426,528	-7.501	-3.2	0.55
Northwestern Sahara Aquifer System	957,574	-2.805	-2.69	0.76
Murzuk-Djado Basin	494,151	-4.275	-2.11	0.5
Lake Chad Basin	1,483,183	-1.042	-1.55	1.26
Sudd Basin (Umm Ruwaba Aquifer)	488,127	-2.855	-1.39	0.53
Indus Basin	313,201	-4.263	-1.34	0.27
Guarani Aquifer System	1,793,747	-0.579	-1.04	1.68
Californian Central Valley Aquifer System	77,917	-8.887	-0.69	0.15
Paris Basin	164,485	-4.118	-0.68	0.24
Taoudeni-Tanezrouft Basin	741,127	-0.496	-0.37	0.48
Ogaden-Juba Basin	1,094,627	-0.335	-0.37	1.16
Tarim Basin	467,140	-0.232	-0.11	0.14

Total (km^3 yr-1)	**-87.3**	**+/- 5.73**
Total (mm yr-1 SLE)	**+0.24**	**+/- 0.02**

To present an estimate of the climate-driven changes in hydrology over the 2002-2014 period, we need to make some assumptions about the human-induced changes in hydrology based on prior information. To form a candidate estimate of human-induced changes over the GRACE record, we could represent groundwater depletion using the mean value of the recently presented studies that coincide with the GRACE period, and the full range of differences between them as a possible uncertainty, noting that the published error on any of these estimates is likely not comprehensive (or in the case of *Doll et al.* (*16*) does not exist). For 2002-2014, we would assume a groundwater depletion number of 0.44 ± 0.13 mm yr^{-1} SLE (i.e. the mean of the values from the literature discussed above). Then we would subtract the other effects (mostly reservoir impundment), assuming a continuation of those trends from 1993-2010 periods of -0.11 ± 0.05 mm yr^{-1} SLE, although this number is also very poorly observed and difficult to verify, with some studies suggesting a recent reversal in sign due to sedimentation (*22*). Propagation of this number leads to a net human-induced rate of 0.33 ±- 0.14 mm yr^{-1} SLE. Because little evidence exists for the validation of these estimates, they remain highly uncertain. The IPCC's (*1*) 1993-2010 estimate of the direct human contributions to sea level was 0.38 ± 0.12 mm yr^{-1}, and the combined net aquifer estimate of *Richey et al.* (*17*) is 0.24 ± 0.02 mm yr^{-1} (also not with comprehensive uncertainties). It is hard to argue that the suite of numbers provided in the recent studies have improved upon the previous estimate since the new estimates fall within the uncertainty range of the IPCC estimate.

In summary, none of the numbers exclude the existence of a strong climate-driven land water storage trend during the study period. We therefore proceed with the previous IPCC estimate in our study here, with the goal of addressing the present gap in the IPCC budget in terms of climate-driven hydrology, and acknowledging that this number may be updated with further research.

References and Notes

1. J. A. Church *et al*., in *Climate Change 2013: The Physical Science Basis. Contribution of Working Group I to the Fifth Assessment Report of the Intergovernmental Panel on Climate Change*, T. F. Stocker *et al.*, Eds. (Cambridge Univ. Press, 2013).

2. J. A. Church *et al*., in *Climate Change 2001: The Physical Scienc Basis. Contribution of Working Group I to the Third Assessment Report of the Intergovernmental Panel on Climate Change*, B.C. Douglas, A. Ramirez, Eds. (Cambridge Univ. Press, 2001).

3. N. L. Bindoff *et al*., in *Climate Change 2007: The Physical Science Basis. Contribution of Working Group I to the Fourth Assessment Report of the Intergovernmental Panel on Climate Change*, S. Solomon *et al.*, Eds. (Cambridge Univ. Press, 2007).

4. D. P. Chambers, J. Wahr, R. S. Nerem, Preliminary observations of global ocean mass variations with GRACE. *Geophys. Res. Lett.* **31**, L13310 (2004). doi:10.1029/2004GL020461

5. B. Wouters, R. E. M. Riva, D. A. Lavallée, J. L. Bamber, Seasonal variations in sea level induced by continental water mass: First results from GRACE. *Geophys. Res. Lett.* **38**, L03303 (2011). doi:10.1029/2010GL046128

6. L. Jensen, R. Rietbroek, J. Kusche, Land water contribution to sea level from GRACE and Jason-1 measurements. *J. Geophys. Res. Oceans* **118**, 212–226 (2013). 10.1002/jgrc.20058 doi:10.1002/jgrc.20058

7. P. C. D. Milly, A. Cazenave, C. Gennero, Contribution of climate-driven change in continental water storage to recent sea-level rise. *Proc. Natl. Acad. Sci. U.S.A.* **100**, 13158–13161 (2003). Medline doi:10.1073/pnas.2134014100

8. T. H. Syed, J. S. Famiglietti, D. P. Chambers, J. K. Willis, K. Hilburn, Satellite-based global-ocean mass balance estimates of interannual variability and emerging trends in continental freshwater discharge. *Proc. Natl. Acad. Sci. U.S.A.* **107**, 17916–17921 (2008).

9. A. Cazenave, H. B. Dieng, B. Meyssignac, K. von Schuckmann, B. Decharme, E. Berthier, The rate of sea-level rise. *Nature Climate Change* **4**, 358–361 (2014). doi:10.1038/nclimate2159

10. A. S. Gardner, G. Moholdt, J. G. Cogley, B. Wouters, A. A. Arendt, J. Wahr, E. Berthier, R. Hock, W. T. Pfeffer, G. Kaser, S. R. Ligtenberg, T. Bolch, M. J. Sharp, J. O. Hagen, M. R. van den Broeke, F. Paul, A reconciled estimate of glacier contributions to sea level rise: 2003 to 2009. *Science* **340**, 852–857 (2013). Medline doi:10.1126/science.1234532

11. A. Shepherd, E. R. Ivins, G. A, V. R. Barletta, M. J. Bentley, S. Bettadpur, K. H. Briggs, D. H. Bromwich, R. Forsberg, N. Galin, M. Horwath, S. Jacobs, I. Joughin, M. A. King, J. T. Lenaerts, J. Li, S. R. Ligtenberg, A. Luckman, S. B. Luthcke, M. McMillan, R. Meister, G. Milne, J. Mouginot, A. Muir, J. P. Nicolas, J. Paden, A. J. Payne, H. Pritchard, E. Rignot, H. Rott, L. S. Sørensen, T. A. Scambos, B. Scheuchl, E. J. Schrama, B. Smith, A. V. Sundal, J. H. van Angelen, W. J. van de Berg, M. R. van den Broeke, D. G. Vaughan, I. Velicogna, J. Wahr, P. L. Whitehouse, D. J. Wingham, D. Yi, D. Young, H. J. Zwally, A reconciled estimate of ice-sheet mass balance. *Science* **338**, 1183–1189 (2012). Medline doi:10.1126/science.1228102

12. B. F. Chao, Y. H. Wu, Y. S. Li, Impact of artificial reservoir water impoundment on global sea level. *Science* **320**, 212–214 (2008). Medline doi:10.1126/science.1154580

13. Y. Wada, L. P. H. van Beek, F. C. S. Weiland, B. F. Chao, Y. H. Wu, M. F. P. Bierkens, Past and future contribution of global groundwater depletion to sea-level rise. *Geophys. Res. Lett.* **39**, L09402 (2012). doi:10.1029/2012GL051230

14. L. F. Konikow, Contribution of global groundwater depletion since 1900 to sea-level rise. *Geophys. Res. Lett.* **38**, L17401 (2011). doi:10.1029/2011GL048604

15. Y. N. Pokhrel, N. Hanasaki, P. J. F. Yeh, T. J. Yamada, S. Kanae, T. Oki, Model estimates of sea-level change due to anthropogenic impacts on terrestrial water storage. *Nat. Geosci.* **5**, 389–392 (2012). doi:10.1038/ngeo1476

16. P. Döll, H. Müller Schmied, C. Schuh, F. T. Portmann, A. Eicker, Global-scale assessment of groundwater depletion and related groundwater abstractions: Combining hydrological modeling with information from well observations and GRACE satellites. *Water Resour. Res.* **50**, 5698–5720 (2014). 10.1002/2014WR015595 doi:10.1002/2014WR015595

17. A. S. Richey, B. F. Thomas, M.-H. Lo, J. T. Reager, J. S. Famiglietti, K. Voss, S. Swenson, M. Rodell, Quantifying renewable groundwater stress with GRACE. *Water Resour. Res.* **51**, 5217–5238 (2015).

18. J. Gonçalvès, J. Petersen, P. Deschamps, B. Hamelin, O. Baba-Sy, Quantifying the modern recharge of the "fossil" Sahara aquifers. *Geophys. Res. Lett.* **40**, 2673–2678 (2013). 10.1002/grl.50478 doi:10.1002/grl.50478

19. M.-H. Lo, J. S. Famiglietti, Irrigation in California's Central Valley strengthens the southwestern U.S. water cycle. *Geophys. Res. Lett.* **40**, 301–306 (2013). 10.1002/grl.50108 doi:10.1002/grl.50108

20. L. F. Konikow, Comment on "Model estimates of sea-level change due to anthropogenic impacts on terrestrial water storage" by Pokhrel *et al*.. *Nat. Geosci.* **6**, 2 (2013).

21. C. Boening, J. K. Willis, F. W. Landerer, R. S. Nerem, J. Fasullo, The 2011 La Niña: So strong, the oceans fell. *Geophys. Res. Lett.* **39**, L19602 (2012).

22. D. Lettenmaier, P. Milly, Land waters and sea level. *Nat. Geosci.* **2**, 452–454 (2009). doi:10.1038/ngeo567

23. B. D. Tapley, S. Bettadpur, J. C. Ries, P. F. Thompson, M. M. Watkins, GRACE measurements of mass variability in the Earth system. *Science* **305**, 503–505 (2004). Medline doi:10.1126/science.1099192

24. I. Velicogna, J. Wahr, Measurements of time-variable gravity show mass loss in Antarctica. *Science* **311**, 1754–1756 (2006). Medline doi:10.1126/science.1123785

25. S. B. Luthcke, A. A. Arendt, D. D. Rowlands, J. J. McCarthy, C. F. Larsen, Recent glacier mass changes in the Gulf of Alaska region from GRACE mascon solutions. *J. Glaciol.* **54**, 767–777 (2008). doi:10.3189/002214308787779933

26. A. S. Gardner, G. Moholdt, B. Wouters, G. J. Wolken, D. O. Burgess, M. J. Sharp, J. G. Cogley, C. Braun, C. Labine, Sharply increased mass loss from glaciers and ice caps in

the Canadian Arctic Archipelago. *Nature* **473**, 357–360 (2011). Medline doi:10.1038/nature10089

27. T. Jacob, J. Wahr, W. T. Pfeffer, S. Swenson, Recent contributions of glaciers and ice caps to sea level rise. *Nature* **482**, 514–518 (2012). Medline doi:10.1038/nature10847

28. G.-Y. Niu, K.-W. Seo, Z.-L. Yang, C. Wilson, H. Su, J. Chen, M. Rodell, Retrieving snow mass from GRACE terrestrial water storage change with a land surface model. *Geophys. Res. Lett.* **34**, L15704 (2009). doi:10.1029/2007GL030413

29. M. Rodell, I. Velicogna, J. S. Famiglietti, Satellite-based estimates of groundwater depletion in India. *Nature* **460**, 999–1002 (2009). Medline doi:10.1038/nature08238

30. J. S. Famiglietti, M. Lo, S. L. Ho, J. Bethune, K. J. Anderson, T. H. Syed, S. C. Swenson, C. R. de Linage, M. Rodell, Satellites measure recent rates of groundwater depletion in California's Central Valley. *Geophys. Res. Lett.* **38**, L03403 (2011). doi:10.1029/2010GL046442

31. H. Kim, P. J.-F. Yeh, T. Oki, S. Kanae, Role of rivers in the seasonal variations of terrestrial water storage over global basins. *Geophys. Res. Lett.* **36**, L17402 (2009). doi:10.1029/2009GL039006

32. G. Ramillien, S. Bouhours, A. Lombard, A. Cazenave, F. Flechtner, R. Schmidt, Land water storage contribution to sea level from GRACE geoid data over 2003-2006. *Global Planet. Change* **60**, 381–392 (2008). doi:10.1016/j.gloplacha.2007.04.002

33. P. C. D. Milly *et al*., in *Understanding Sea-Level Rise and Variability*, J. A. Church, P. L. Woodworth, T. Aarup, W. S. Wilson, Eds. (Wiley-Blackwell, 2010), pp. 226–255.

34. W. Llovel, M. Becker, A. Cazenave, J.-F. Crétaux, G. Ramillien, Global land water storage change from GRACE over 2002-2009; Inference on sea level. *C. R. Geosci.* **342**, 179–188 (2010). doi:10.1016/j.crte.2009.12.004

35. R. Rietbroek, S.-E. Brunnabend, J. Kusche, J. Schroeter, C. Dahle, Revisiting the contemporary sea-level budget on global and regional scales. *Proc. Natl. Acad. Sci. U.S.A.* 10.1073/pnas.1519132113 (2015).

36. M. M. Watkins, D. N. Wiese, D.-N. Yuan, C. Boening, F. W. Landerer, Improved methods for observing Earth's time variable mass distribution with GRACE using spherical cap mascons. *J. Geophys. Res. Solid Earth* **120**, 2648–2671 (2015). doi:10.1002/2014JB011547

37. W. R. Peltier, D. F. Argus, R. Drummond, Space geodesy constrains ice age terminal deglaciation: The global ICE-6G_C (VM5a) model. *J. Geophys. Res. Solid Earth* **120**, 450–487 (2015). doi:10.1002/2014JB011176

38. M. Cheng, B. D. Tapley, Variations in the Earth's oblateness during the past 28 years. *J. Geophys. Res.* **109** (B9), B09402 (2004). doi:10.1029/2004JB003028

39. J. Wahr, R. S. Nerem, S. V. Bettadpur, The pole tide and its effect on GRACE time-variable gravity measurements: Implications for estimates of surface mass variations. *J. Geophys. Res. Solid Earth* **120**, 4597–4615 (2015).

40. S. Swenson, D. Chambers, J. Wahr, Estimating geocenter variations from a combination of GRACE and ocean model output. *J. Geophys. Res.* **113** (B8), B08410 (2008). doi:10.1029/2007JB005338

41. S.-C. Han, R. Riva, J. Sauber, E. Okal, Source parameter inversion for recent great earthquakes from a decade-long observation of global gravity fields. *J. Geophys. Res. Solid Earth* **118**, 1240–1267 (2013). doi:10.1002/jgrb.50116

42. R. Riva, J. Bamber, D. Lavallee, B. Wouters, Sea-level finger-print of continental water and ice mass change from GRACE. *Geophys. Res. Lett.* **37**, L19605 (2010). doi:10.1029/2010GL044770

43. W. Llovel, J. K. Willis, F. W. Landerer, I. Fukumori, Deep-ocean contribution to sea level and energy budget not detectable over the past decade. *Nature Climate Change* **4**, 1031–1035 (2014). doi:10.1038/nclimate2387

44. Materials and methods are available as supplementary materials on *Science* Online.

45. J. T. Reager, B. F. Thomas, J. S. Famiglietti, River basin flood potential inferred using GRACE gravity observations at several months lead time. *Nat. Geosci.* **7**, 588–592 (2014). doi:10.1038/ngeo2203

46. J. L. Chen, C. R. Wilson, B. D. Tapley, The 2009 exceptional Amazon flood and interannual terrestrial water storage change observed by GRACE. *Water Resour. Res.* **46**, W12526 (2010). doi:10.1029/2010WR009383

47. G. Ramillien, F. Frappart, L. Seoane, Application of the regional water mass variations from GRACE Satellite Gravimetry to large-scale water management in Africa. *Remote Sens.* **6**, 7379–7405 (2014). doi:10.3390/rs6087379

48. E. Forootan, J. Kusche, I. Loth, W.-D. Schuh, A. Eicker, J. Awange, L. Longuevergne, B. Diekkrüger, M. Schmidt, C. K. Shum, Multivariate prediction of total water storage changes over West Africa from multi-satellite data. *Surv. Geophys.* **35**, 913–940 (2014). doi:10.1007/s10712-014-9292-0

49. J. T. Reager, J. S. Famiglietti, Global terrestrial water storage capacity and flood potential using GRACE. *Geophys. Res. Lett.* **36**, L23402 (2009). 10.1029/2009GL040826 doi:10.1029/2009GL040826

50. J. T. Fasullo, C. Boening, F. W. Landerer, R. S. Nerem, Australia's unique influence on global sea level in 2010–2011. *Geophys. Res. Lett.* **40**, 4368–4373 (2013). doi:10.1002/grl.50834

51. K. A. Voss, J. S. Famiglietti, M. H. Lo, C. de Linage, M. Rodell, S. C. Swenson, Groundwater depletion in the Middle East from GRACE with implications for transboundary water management in the Tigris-Euphrates-Western Iran region. *Water Resour. Res.* **49**, 904–914 (2013). Medline doi:10.1002/wrcr.20078

52. E. Forootan, R. Rietbroek, J. Kusche, M. A. Shari, J. L. Awange, M. Schmidt, P. Omondi, J. Famiglietti, Separation of large scale water storage patterns over Iran using GRACE, altimetry and hydrological data. *Remote Sens. Environ.* **140**, 580–595 (2014). 10.1016/j.rse.2013.09.025 doi:10.1016/j.rse.2013.09.025

53. B. R. Scanlon, L. Longuevergne, D. Long, Ground referencing GRACE satellite estimates of groundwater storage changes in the California Central Valley, USA. *Water Resour. Res.* **48**, W04520 (2012). doi:10.1029/2011WR011312

54. B. R. Scanlon, C. C. Faunt, L. Longuevergne, R. C. Reedy, W. M. Alley, V. L. McGuire, P. B. McMahon, Groundwater depletion and sustainability of irrigation in the US High Plains and Central Valley. *Proc. Natl. Acad. Sci. U.S.A.* **109**, 9320–9325 (2012). Medline doi:10.1073/pnas.1200311109

55. W. Feng, M. Zhong, J.-M. Lemoine, R. Biancale, H.-T. Hsu, J. Xia, Evaluation of groundwater depletion in North China using the Gravity Recovery and Climate Experiment (GRACE) data and ground-based measurements. *Water Resour. Res.* **49**, 2110–2118 (2013). doi:10.1002/wrcr.20192

56. F. Flechtner, H. Dobslaw, E. Fagiolini, AOD1B Product Description Document for Product Release 05, GRACE 327-750, Rev 4.3 (2015).

57. A. Paulson, S. Zhong, J. Wahr, Inference of mantle viscosity from GRACE and relative sea level data. *Geophys. J. Int.* **171**, 497–508 (2007). doi:10.1111/j.1365-246X.2007.03556.x

58. S. Swenson, J. Wahr, Methods for inferring regional surface-mass anomalies from Gravity Recovery and Climate Experiment (GRACE) measurements of time-variable gravity. *J. Geophys. Res.* **107** (B9), 2193 (2002). 10.1029/2001JB000576 doi:10.1029/2001JB000576

59. X. Wu, M. B. Heflin, H. Schotman, B. L. A. Vermeersen, D. Dong, R. S. Gross, E. R. Ivins, A. W. Moore, S. E. Owen, Simultaneous estimation of global present-day water transport and glacial isostatic adjustment. *Nat. Geosci.* **3**, 642–646 (2010). doi:10.1038/ngeo938

60. W. R. Peltier, Global glacial isostasy and the surface of the ice-age Earth: The ICE-5G (VM2) model and GRACE. *Annu. Rev. Earth Planet. Sci.* **32**, 111–149 (2004). doi:10.1146/annurev.earth.32.082503.144359

61. J. Wahr, S. Zhong, Computations of the viscoelastic response of a 3-D compressible Earth to surface loading: An application to glacial isostatic adjustment in Antarctica and Canada. *Geophys. J. Int.* **192**, 557–572 (2013). doi:10.1093/gji/ggs030

62. W. T. Pfeffer, A. A. Arendt, A. Bliss, T. Bolch, J. G. Cogley, A. S. Gardner, J.-O. Hagen, R. Hock, G. Kaser, C. Kienholz, E. S. Miles, G. Moholdt, N. Mölg, F. Paul, V. Radić, P. Rastner, B. H. Raup, J. Rich, M. J. Sharp, The Randolph Glacier Inventory: A globally complete inventory of glaciers. *J. Glaciol.* **60**, 537–552 (2014). doi:10.3189/2014JoG13J176

63. J. G. Cogley, Geodetic and direct mass-balance measurements: Comparison and joint analysis. *Ann. Glaciol.* **50**, 96–100 (2009). doi:10.3189/172756409787769744

64. I. Sasgen, M. van den Broeke, J. L. Bamber, E. Rignot, L. S. Sørensen, B. Wouters, Z. Martinec, I. Velicogna, S. B. Simonsen, Timing and origin of recent regional ice-mass loss in Greenland. *Earth Planet. Sci. Lett.* **333–334**, 293–303 (2012).

65. E. J. O. Schrama, B. Wouters, R. Rietbroek, A mascon approach to assess ice sheet and glacier mass balances and their uncertainties from GRACE data. *J. Geophys. Res. Solid Earth* **119**, 6048–6066 (2014). doi:10.1002/2013JB010923

66. I. Sasgen, H. Konrad, E. R. Ivins, M. R. Van den Broeke, J. L. Bamber, Z. Martinec, V. Klemann, Antarctic ice-mass balance 2003 to 2012: Regional reanalysis of GRACE satellite gravimetry measurements with improved estimate of glacial-isostatic adjustment based on GPS uplift rates. *Cryosphere* **7**, 1499–1512 (2013). doi:10.5194/tc-7-1499-2013

67. R. F. Adler, G. J. Huffman, A. Chang, R. Ferraro, P.-P. Xie, J. Janowiak, B. Rudolf, U. Schneider, S. Curtis, D. Bolvin, A. Gruber, J. Susskind, P. Arkin, E. Nelkin, The Version 2 Global Precipitation Climatology Project (GPCP) Monthly Precipitation Analysis (1979 - Present). *J. Hydrometeorol.* **4**, 1147–1167 (2003). doi:10.1175/1525-7541(2003)004<1147:TVGPCP>2.0.CO;2

68. T. Ngo-Duc, K. Laval, J. Polcher, A. Lombard, A. Cazenave, Effects of land water storage on global mean sea level over the past half century. *Geophys. Res. Lett.* **32**, L09704 (2005). doi:10.1029/2005GL022719

69. S. I. Seneviratne, M. G. Donat, B. Mueller, L. V. Alexander, No pause in the increase of hot temperature extremes. *Nature Climate Change* **4**, 161–163 (2014). doi:10.1038/nclimate2145